Volume 1 | Number 1 | Jan 2013 | Pages 1–100

MedChemComm

www.rsc.org/medchemcomm

pDOS

pFLT3

FLT3

ROYAL SOCIETY OF CHEMISTRY

EFMC
European Federation
for Medicinal Chemistry

ROYAL SOCIETY OF CHEMISTRY

www.rsc.org/medchemcomm

Journal Name

ARTICLE

In silico study on aging and reactivation processes of tabun conjugated AChE

Nellore Bhanu Chandar,[a,b] Rabindranath Lo,[a] Manoj K. Kesharwani[a] and Bishwajit Ganguly*[a,b]

We have examined the aging and reactivation mechanisms of the tabun-conjugated AChE using MP2/6-31+G*//M05-2X/6-31G* level of theory. The activation barriers have been calculated for the aging process considering both O-dealkylation and deamination (P-N anti deamination and rearrangement-deamination) pathways. Aging process is reported as competing course with the reactivation process as the deamination/dealkylation process occurs rapidly with half-life (<1-30 min) depending on the enzyme. To avoid the aging process, suitable reactivators are in demand to restore the function of AChE. 3-hydroxy-2-Pyridylamide oxime (amidoxime (I)) has been chosen as reactivator to examine the competing aging process of tabun-conjugated AChE. The energy of activation predicted for the reactivation of tabun-conjugated AChE by 3-hydroxy-2-Pyridylamide oxime (amidoxime (I)) is 2.3 kcal/mol, which is lower than the activation energies calculated for studied aging processes. The structural analysis from the docking studies of the model oxime (I) and the oximes used for the reactivation of tabun-inhibited AChE reveal that the peripheral sites play an important role for the efficacy of drugs. The reactivator is stabilized by π-π interaction with Tyr337, and edge to face (C-H…π) interaction with Trp86 residues and hydrogen bonding interactions with His447 and alkoxy oxygen of tabun in the active site of tabun-inhibited AChE. Such stabilization from surrounding aromatic residues is helpful for favourable orientation of oxime group towards the phosphorus centre of tabun. The calculated LogP value indicates that the neutral reactivator can effectively penetrate through the blood brain barrier. The calculated results show that the neutral antidotes can effectively reactivate the tabun-inhibited AChE prior to its aging process.

Introduction

Nerve agent tabun inhibits acetylcholinesterase by phosphorylating a serine hydroxyl group (ser203 in *m*AChE), which is directly responsible for the hydrolysis of the neurotransmitter acetylcholine. The phosphorus conjugate of the tabun-inhibited AChE may further undergo an elimination reaction, known as "aging": two alternative pathways have been proposed for the aging mechanism of tabun-inhibited AChE. One mechanism involves P-N bond cleavage called deamination process[1-2] and the other involves O-C bond breaking leads to elimination of alkylate (i.e. O-dealkylation process).[3] Both mechanisms were suggested involving the use of mass spectrometry (MS) and crystallographic technique.

The first X-ray crystal structure of aged tabun-inhibited AChE was reported with mouse AChE.[4] The structural data of aged AChE revealed that the aging follows the deamination pathway through the breaking of P-N bond by the nucleophilic attack of water. Mass spectrometric analysis performed to examine the aging process of tabun and butyl tabun adducts also suggests that the aging process undergoes though P-N bond scission. Both these adducts show a mass decrease of 28±4 Da.[1] However, recent report with the mass spectrometric study shows that the P-N bonds of Sp-tabun thiocholine adduct are stable at pH= 8 during trypsin digestion, but is labile at pH= 2 in pepsin digestion conditions.[5] This report suggests that observed P-N scission of tabun-adduct in MS analysis was due to acid labile P-N bond, instead of enzyme-catalyzed aging mechanism.[5]

Moreover, the reinterpretation of the crystal structural data of the aged *m*AChE suggests that the aging process occurs through the dealkylation of the ethoxy group instead of deamination of dimethylamine.[3] Furthermore, the crystallographic studies of tabun-inhibited *h*BChE suggested O-dealkylation of ethoxy group.[3,6] In O-dealkylation mechanism, His447 imidazolium stabilizes a negative charge on the C-O$^{\delta-}$ oxygen of ethoxy substituent of tabun-inhibited AChE conjugates. Glu202 residue activates the water molecule by abstracting the hydrogen to form hydroxide ion, which can

further attack on the carbocationic center ($C^{\delta+}$-O of carbon). This leads to the O-C bond cleavage and release of ethoxy group.[6]

Further, Nachon et al. has suggested with x-ray crystal structure data that substitution based mechanism for aging can occur through the deamination pathway by the rearrangement of the trigonal-bipyramidal transition state for *hB*ChE conjugates analogue of tabun.[7] The crystal structures reports of inhibited *h*BChE by different *N*-monoalkyl and *N,N*-dialkyl tabun analogues suggest that the aging process can be progressed either via dealkylation or deamidation, depending on the OP structure.[7,8]

The O-dealkylation and P-N deamination of aging processes of tabun-conjugated AChE have been examined using quantum chemical calculations with B3LYP/6-31+G* level of theory.[9] The computational results revealed that the O-dealkylation aging mechanism of tabun-AChE conjugate proceeds via one step S_N2 process, while P-N deamination mechanism proceeds via two step addition-elimination reaction at the phosphorus center of tabun-AChE conjugate. The P-N bond breaking deamination mechanism is preferred via newly proposed rearrangement process.[7]

In most of the reports, oximes were treated as a single entity for the reactivation of OPs-inhibited AChE without considering the aging propensity of the phosphorylated AChE.[10] However, generally the reactivation of OPs-inhibited AChE is also a competing process with aging of OPs-inhibited AChE. It is known that the aging process is irreversible in nature and AChE cannot be functional with the reactivators.[11-13] An earlier study on aging and reactivation mechanisms of tabun-inhibited AChE using quantum mechanical/molecular mechanical method[14] reports a comparative study of these two processes with the help of the relative energy barrier of HLÖ-7 induced reactivation and O-C bond breaking (O-dealkylation) aging process.

In this article, we have performed quantum chemical calculations on aging and reactivation processes of tabun-inhibited AChE with 3-hydroxy-2-Pyridylamide oxime (amidoxime (I)) as neutral reactivator (Scheme 1). The experimental and theoretical studies have shown that the charged drug shows lower tendency to cross BBB for effective,[15-17] whereas the synthesized non-ionic drugs can easily penetrate the BBB and found to show high potency towards reactivation of OPs-inhibited AChE.[18-20] Amidoxime (I) is a neutral α-nucleophile which has been used successfully for the hydrolysis/reactivation of organophosphorus nerve (OPN) agents VX.[21-23] The success of amidoxime (I) in V-type of OPN hydrolysis, this oxime has been selected in this present study to examine its efficacy against tabun-inhibited AChE. In a report, the amidoximes and aldoximes have been used for the reactivation of tabun-inhibited AChE.[23] The reactivations with such oximes varied with the nature of the alkyl chain lengths and peripheral sites. In addition to that polyacrylamidoxime (PANOx) and poly(N-hydroxyacrylamide) have also been reported for degradation processes of the chemical warfare

agents like GB (sarin), GD (soman) and VX in non-enzymatic conditions.[24]
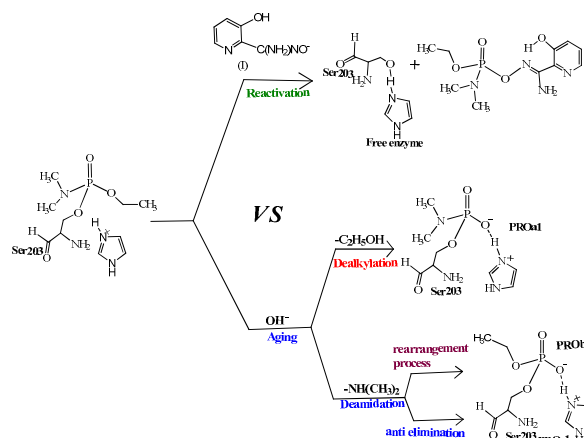
Scheme 1: Schematic representation of possible aging pathways and reactivation pathway of OP-conjugated AChE.

Computational Methodology

Tabun-conjugated serine (SUN) residue with protonated His447 imidazole ring was modeled from the PDB structure of tabun-conjugated mouse acetylcholinesterase (PDB code: 2JF0).[25] This modelled tabun-inhibited AChE adduct was optimized at M05-2X/6-31G* level of theory in aqueous medium.[26] All calculations were performed with Gaussian 09 suite program.[27] The geometry optimizations of all stationary points were carried out in aqueous phase at M05-2X/6-31G* energy level with polarizable continuum solvation model (PCM) using the integral equation formalism variant (IEF-PCM).[28,29] Single point energies are calculated at the MP2/6-31+G* level of theory to get accurate energies using M05-2X/6-31G* optimized geometries.[30]

The frequency calculations have been performed for all the stationary points to verify that the transition structures had single, imaginary frequency. The intrinsic reaction coordinate (IRC) calculations of the saddle points connect two minima in both directions by following the eigenvectors associated to the unique negative eigenvalue of the Hessian matrix, using the González and Schlegel integration method.[31] We have calculated Natural bond orbital (NBO) for 3-hydroxy-2-pyridine aldoxime and 3-hydroxy-2-Pyridylamide oxime (amidoxime (I)).[32]

Further, We have performed docking study by using PDB code: 2JF0 crystal structure, which is complexed of Ortho-7 reactivator and tabun-inhibited *m*AChE conjugate. Using the Macromodel program, we have added hydrogen's and minimized of drug-protein complex.[33] For minimization of the protein system, we have used MMFF force field and PRCG method. Further minimized protein was considered for the docking study. The docking study have been performed by using a grid based Autodock 4.2 program.[34] We have performed simulations with AutoDock using six spatial degrees of freedom such as rotation and translation along with torsional

degrees of freedom. To reach global minimum, we have evaluated interaction energy at each step. To explore the grid space and perform energy evaluations of the position of the ligand with respect to the target energy grids we have employed Lamarckian Genetic Algorithm (LGA). The grid map prepared by using grid box with 70-70-70 Å. Finally for calculating the docking possibilities we have used the genetic algorithm with local search (GALS). Furthermore, we have calculated LogP value of amidoxime (I) by using PrologP module of Pallas 3.8.1.2 software.[35]

Results and discussion

The MP2/6-31+G*//M05-2X/6-31G* level of theory has been employed in this work to study the aging mechanism of tabun conjugated serine (SUN) via dealkylation process (breaking of O-C bond) and deamination process (breaking of P-N bond). The potential energy surface diagrams and optimized geometries for O-dealkylation, P-N anti deamination and P-N rearrangement-deamination processes are shown in Figs. 1-6. The OH$^-$ ion that initiates the nucleophilic attack on phosphorus centre or carbocationic centre (C$^{\delta+}$-O of carbon) in the aging process is produced from activation of water through interacting with Glu202 and the catalytic triad histidine (His447) of AChE.[6] According to Nachon et al, it should be expected that the aging reaction proceeds favourably in the presence of protonated histidine.[7] In earlier report, the theoretical calculations show that the incorporation of imidazole group of catalytic residue His447 lowers the activation free energy of the aging process.[9] In this study, we have considered imidazolium group of histidine in the aging process.

O-dealkylation aging mechanism

We have examined the O-C bond breaking process in aging mechanism using protonated histidine instead of neutral histidine.[9,36] The O-dealkylation aging of tabun-conjugated AChE proceeds in S$_N$2 type mechanism with the activation barrier 9.80 kcal/mol (Fig. 1). Such process leads to the breaking of O-C bond and release of ethoxy group (Fig. 2). The crystallographic and theoretical studies on tabun-inhibited AChE also infer such O-dealkylation mechanism during the aging process.[3,6] The optimized geometries of transition state (TSa) and products (PROa1 and ethanol) are given in Fig. 2. The TS geometry shows that the calculated bond distances are 1.72 Å and 2.24 Å for O-C$_{ethoxy}$ and C-O$_{hydroxy}$ in the concerted transition state TSa (Fig. 2). The formation of the products (PROa1 and ethanol) from O-dealkylation process is 40.4 kcal/mol lower in energy than complex-a (Fig. 2). In the product PROa1, the protonated histidine forms salt-bridge with the negatively charged alkoxy oxygen of tabun-inhibited serine adduct. In the presence of unprotonated histidine similar hydrogen bonding has also been found to stabilize the aged product.[9] The N-H···O distance becomes shorter in product PROa1 (1.53 Å) compared to the transition state TSa (1.76 Å). (Fig. 2)
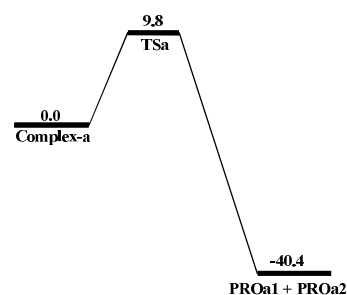
Fig. 1. MP2/6-31+G*//M05-2X/6-31G* calculated energy profile diagram for O-deakylation of tabun-conjugated AChE in aqueous phase. Relative energies are in kcal/mol.
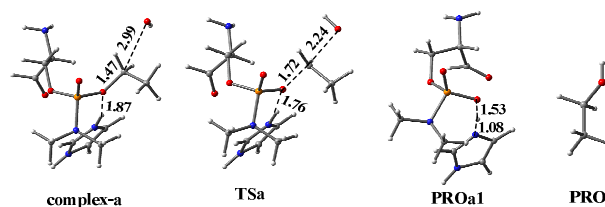
Fig. 2. M05-2X/6-31G* optimized geometries and selected bond distances in Å for species involved in O-dealkylation of tabun-conjugated AChE in aqueous phase (grey= carbon, blue = nitrogen, white = hydrogen, orange= phosphorus and red = oxygen)

Earlier crystallographic and mass spectrometric (MS) analyses of aged tabun-inhibited AChE suggested the deamination aging process of the inhibited AChE enzyme. In general, the deamination process proceeds through two different pathways: direct anti deamination and rearrangement-deamination processes.

P-N anti-deamination aging mechanism

First, we have examined the aging process in P-N anti elimination manner. The anti P-N deamination proceeds via two-step addition-elimination reaction mechanism and the nucleophilic attack of OH$^-$ ion on phosphorus centre is the rate determining step (TSb1) with 3.1 kcal/mol energy of activation (Fig. 3). In this anti deamination mechanism, the OH$^-$ ion attacks the phosphorus center opposite to dimethylamine group at apical positions due to weaker and longer bond between phosphorus and apical atoms.[37] Therefore, the P-N bond cleavage is favoured at apical position in such that the attacking OH$^-$ and the leaving dimethylamine group are in 180º to each other. Furthermore, the product (PROb1) forms aged product through second transition state TSb2, with 1.9 kcal/mol energy of activation by leaving amine group (PROb2) from tabun-conjugated AChE (Figs 3 and 4). The calculated results also show that there is an instantaneous proton transfer occurs in PROb1 from hydroxyl oxygen to the nitrogen of histidine moiety with a very low energy barrier (Fig. S1). Furthermore, in the presence of full enzymatic condition, the stable aged product PROb3 can adjust to another protonated product PROb4 with the help of surrounding residues and solvent molecules. However, in isolated state PROb4 is energetically

less stable than PROb3 by 2.5 kcal/mol (Figs.S1 and S2 in Supplementary Information).
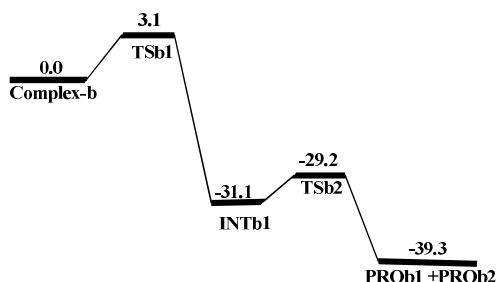
Fig. 3. MP2/6-31+G*//M05-2X/6-31G* calculated energy profile diagram for deamination (P-N anti elimination) of tabun-conjugated AChE in aqueous phase. Relative energies are in kcal/mol.
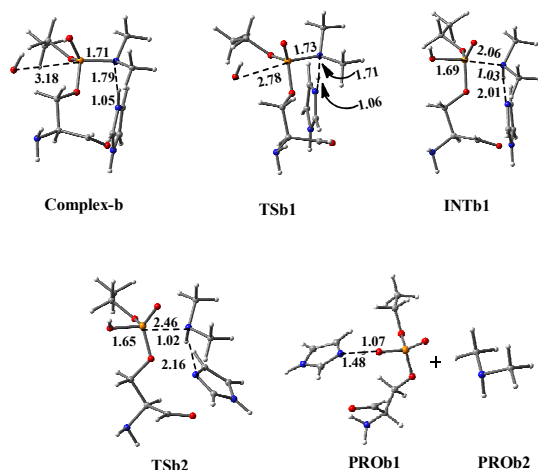
Fig. 4. M05-2X/6-31G* optimized geometries and selected bond distances in Å for species involved in deamination (P-N anti elimination) of tabun-conjugated AChE in aqueous phase (grey= carbon, blue = nitrogen, white = hydrogen, orange= phosphorus and red = oxygen)

P-N rearrangement-deamination aging mechanism

We have also examined the possibility of the aging process through the rearrangement pathway. Such rearrangement process was proposed by Nachon et al. and the reaction pathways have been shown by theoretical calculations in the presence of unprotonated histidine moiety.[7,9] The P-N rearrangement deamination aging is a three-step process in the presence of protonated histidine, where the attacking OH⁻ and ethoxy group are in apical positions (i.e. 90º to the leaving dimethylamine group).[7,9] This leads to addition transition state TSc1 with 3.6 kcal/mol energy of activation resulted into trigonal bipyramidal intermediate INTc1. (Figs. 5 and 6) Furthermore, the INTc1 undergoes internal rearrangement through TSc2 by Berry pseudorotation with the energy of 6 kcal/mol to INTc2 so that the leaving group (dimethylamine group). (Figs. 5 and 6) In the transition state TSc3 the protonated histidine stabilizes the hydroxyl oxygen by electrostatic stabilization. (Fig. 6)
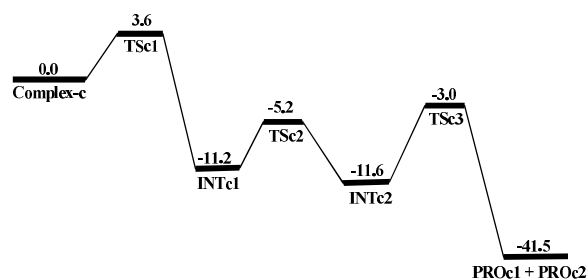
Fig. 5. MP2/6-31+G*//M05-2X/6-31G* calculated energy profile diagram for deamination (P-N rearrangement-deamnation process) of tabun-conjugated AChE in aqueous phase. Relative energies are in kcal/mol.
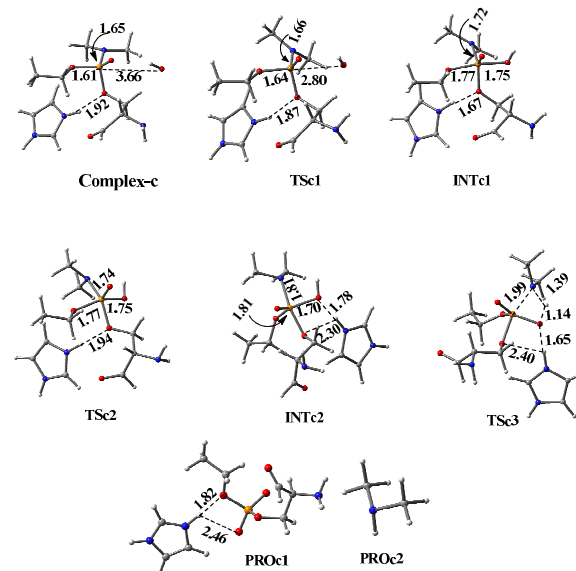
Fig. 6. M05-2X/6-31G* optimized geometries and selected bond distances in Å for species involved in deamination (P-N rearrangement-deamination process) of tabun-conjugated AChE in aqueous phase (grey= carbon, blue = nitrogen, white = hydrogen, orange= phosphorus and red = oxygen).

The calculated results show that the activation energy barriers for P-N anti deamination and P-N rearrangement deamination are energetically close and in both cases the nucleophilic addition of hydroxide on the phosphorus of phosphate is the rate determine step. Comparing the potential energy profiles and stable products formed by O-dealkylation and P-N deamination processes, the calculated results show that P-N deamination mechanism is a catalytic control process and most favoured mechanism for the aging of tabun-inhibited AChE using model systems. However, these results are not in accord to crystal structure based reported aging mechanism, which suggests for O-dealkylation aging process.[3] It is to note that our results based on modeled systems, rather than considering the whole protein environment. The structural data of non-aged tabun-*h*BChE reveals that the dimethylamine group positioned in the acyl binding pocket, when the enzyme is inhibited by P(R)-tabun.[3] Such arrangement allows the ethoxy substituent to be positioned in the chloine binding pocket for facile dealkylation in the aging process. If the aging process passes through the deamination pathway, then there would have been

relocation of the substituents around the phosphorus after aging process, as the dimethylamine moiety was located in the acyl-binding pocket.[3] Such types of movements are less likely in a constrained active-site pocket like that of *m*AChE.[3] However, in the case of tabun-analogues TA4, the O-ethoxy substituent is situated in the acyl-binding pocket and the shorter *N*-methyl chain placed towards the choline-binding pocket.[7,9] Such arrangement is favourable for the deamination process. These crystallographic studies indicate that the departure of the substituent in the choline-binding pocket for the aging process depends upon the steric and electronic environments. The absence of the protein environment in these calculations is presumably the reason for the discrepancy with the earlier reports.[3] However, it is important to mention to assess the suitability of a reactivator that can reactivate the tabun-inhibited AChE prior to the aging process. The results of our calculations also suggest that the protonated histidine plays crucial role in catalytic stabilization of complex conjugates ions in the aging processes of O-dealkylation, P-N anti deamination and P-N rearrangement deamination mechanisms.

Prior to the aging process, the OP-inhibited AChE can be reactivated by various charged and neutral nucleophilic compounds such as oximes, hydroxamates.[17-20] The reactivation of OP-inhibited AChE is crucial as the aging process starts competing with the former process. In general the rate of aging process is very much fast and the half-time of aging ranges from a few minutes to several days.[38-40] Therefore, there is a demand of efficient antidotes for the reactivation process of OP poisoning in fast aging process. We have examined the reactivation process with an uncharged reactivator (amidoxime (I)) kinetically as well as structurally and compared the calculated results with the studied aging processes.

Reactivation of tabun-inhibited AChE

To examine the efficiency of amidoxime (I) in tabun-inhibited AChE, we have performed MP2/6-31+G*//M05-2X/6-31G* calculations to examine the mechanism of reactivation of tabun-inhibited AChE conjugates by using amidoxime (I) as reactivator as shown in Figs 7 and 8. Amidoxime (I) is selected in this study for two reasons: firstly, because it is a neutral α-nucleophile and the uncharged oxime reactivators have shown the promise with improved lipophilicity and BBB permeability.[17-20] Secondly, it has been used successfully for the hydrolysis/reactivation of organophosphorus nerve (OPN) agents such as VX.[22,23]

To identify the stable structure of 3-hydroxy-2-Pyridylamideoxime, different possible geometries have been optimized with M05-2X/6-31G* level of theory. The calculated results show that amidoxime (I) is energetically more stable than the other geometries due to presence of strong intramolecular hydrogen bonding between OH and oxime nitrogen (Fig. 9). These results correlate well with the available X-ray crystal structure.[21]

The reactivation process proceeds via two-step addition-elimination reaction mechanism and the nucleophilic attack of amidoxime (I) reactivator on phosphorus centre resulted into

trigonal bipyramidal intermediate INTd1 through TSd1 with 2.3 kcal/mol energy of activation (Fig. 7), thus TSd1 is the rate determining step. The trigonal bipyramidal intermediate (INTd1) is lower by 2.4 kcal/mol compared to the energy of complex-d. The INTd1 yields stable activated serine stabilized by His447 and phosphorylated-oxime complex product through a second transition state TSd2, with 1.7 kcal/mol energy of activation. The P-O$_{(amidoxime (I))}$ and P-O$_{(serine)}$ bond distances are 2.43 Å and 1.69 Å for TSd1, 1.80 Å and 1.83 Å for INTd1, 1.65 Å and 3.41 Å for TSd2 respectively. The activation energy calculated for amidoxime (I) reactivation of tabun-inhibited AChE conjugate in this study is slightly lower than other neutral oximes reactivators (3-hyroxyl-2-pyridinealdoxime and deazapralidoxime) reported in earlier work.[15] Such α-hydroxyl pyridylamide oxime derivative shows efficient and selective cleavage of the P-S bond in organophosphorus nerve agent.[21,22] The role of ortho-hydroxyl group in pyridyloximes towards significant enhancing the hydrolysis process has already been reported. The presence of electron donating (NH$_2$) group at oxime group carbon substitution augments the nucleophilicity of the active oxygen atom. To investigate the effect of -NH$_2$ on active oxygen (IV), we have analyzed NBO charges of aldoxime (IV) and amidoxime (I), it's showing that NH$_2$ group added geometry has more negative charges on active oxygen (Fig. 10). These results indicate that -NH$_2$ group enhances the nucleophilicity of the α-nucleophile (IV). Recent reports suggest that aldoxime (IV) and amidoxime (I) can exhibit the reactivation of VX-inhibited hAChE one order of magnitude higher than that displayed by 2-PAM.[21,23] Also, *in vitro* reactivation of tabun-inhibited hAChE with aldoxime (IV) and amidoxime (I) nucleophilic sites showed that the former oxime is a better reactivator in this case.[23]
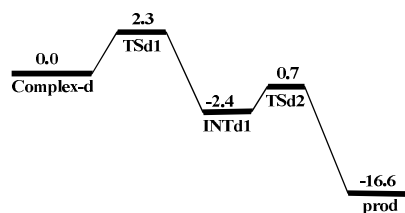
Fig. 7. The potential energy surface for reactivation process of tabun-inhibited AChE conjugate at MP2/6-31+G*//M05-2X/6-31G* level of theory in aqueous phase. Relative energies are given in kcal/mol.
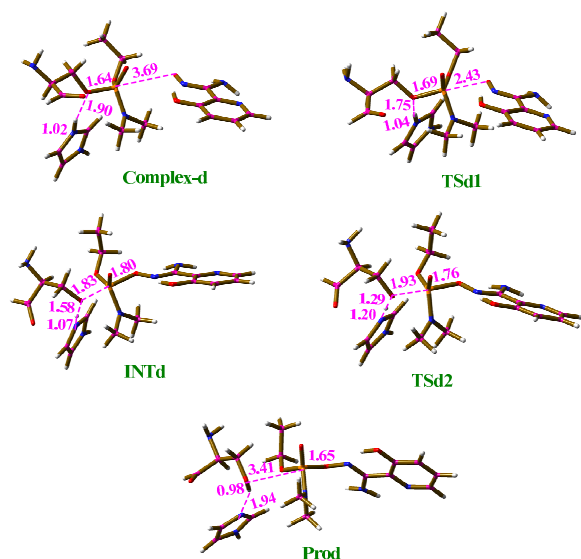
Fig. 8. The optimized geometries and distances are in Å for reactivation process of tabun-inhibited AChE conjugate at M05-2X/6-31G* level in aqueous phase. (red = oxygen, brown = carbon, blue = nitrogen, white = hydrogen)
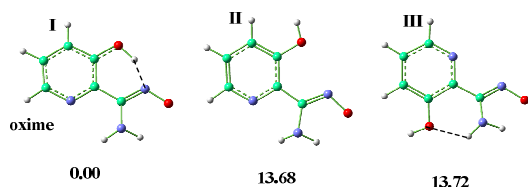
Fig. 9. M05-2X/6-31G* optimized geometries in aqueous phase of various possible conformers of 3-hydroxy-2-Pyridylamide oxime (amidoxime (I)) and their relative energies in kcal/mol at MP2/6-31+G*//M05-2X/6-31G* level of theory. (red = oxygen, green = carbon, blue = nitrogen, white = hydrogen)
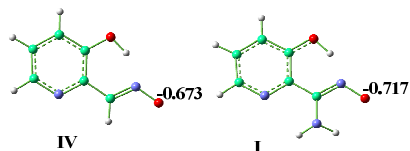
Fig. 10. Optimized geometries in aqueous phase of aldoxime (IV), amidoxime (I) and their NBO charges of active oxygen at M05-2X/6-31G* level of theory. (red = oxygen, green = carbon, blue = nitrogen, white = hydrogen)

The potential energy diagram shows that the activation energy barrier of aging processes are higher than reactivation process (2.3 kcal/mol) involving amidoxime (I). From the overall study it can be concluded that reactivation mechanism will be preferred kinetically over aging process. Earlier report on the reactivation of tabun-inhibited AChE with pyridaldoxime compared with the aging process also showed that the later process is much slower in this case.[41]
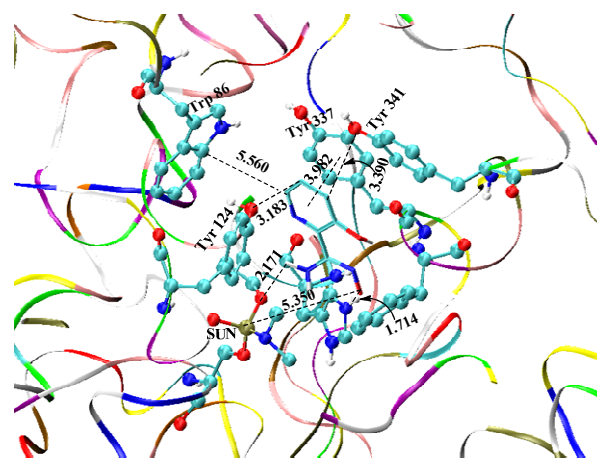
Fig. 11. Stable conformation of amidoxime (I) with tabun-inhibited AChE showing interactions in the active site gorge. (red = oxygen, cyan = carbon, blue = nitrogen, white = hydrogen) (surrounding aromatic residues and SUN are shown in CPK and amidoxime (I) shown in tube format) (Distances are given in Å).

To achieve the effective reactivation process, the nucleophilicity and the orientation of nucleophile reactivator should be crucial in the active site of OP-inhibited AChE.[13] The NBO charge calculation and the kinetic study of the reactivation process with tabun-inhibited AChE conjugates by amidoxime (I) suggested efficient nucleophilic character of the reactivator oxime. Furthermore, to examine the orientation of nucleophile in the active site, we have performed docking study by using autodock 4.2 program.[34] The available crystal geometry of tabun-inhibited AChE shows that after inhibition process, the side chains of His447 and Phe338 push towards Tyr341or Tyr124 at the active site of AChE and it created difficulty for approaching the incoming nucleophilic oxime for reactivation process.[4,25] Thus, the steric hindrance at phosphorus center and weak electrophilicity of phosphorus atom leads to less reactivation in the tabun-inhibited AChE adduct with most of the oximes.[10,42] For better understanding of the structural orientation of amidoxime (I) in the active site gorge, we have performed docking study with the crystal structure of tabun-inhibited AChE (pdb code: 2JF0). The distance between nucleophilic oxygen of amidoxime (I) and electrophilic phosphorus of SUN is 5.350 Å, this distance indicates that it's considerable distance for complex formation of nucleophile and electrophile. In the crystal structure of tabun-inhibited AChE complexed with ortho-7(PDB code no: 2JF0), the distance of nucleophile and electrophile is found to be 6.74 Å.[25] Furthermore, the pyridine ring of amidoxime (I) is stabilized at the active site by forming π-π stacking interactions with Tyr337 and edge to face (C-H…π) interaction with Trp86 residues. Additionally the aromatic ring of amidoxime (I) is stabilized by forming the hydrogen bonds with hydroxyl group of Tyr124 and Tyr341. The substituted amine group of amidoxime (I) generated strong hydrogen bond with alkoxy oxygen of SUN (Fig. 11). Furthermore, the docking results show that the oxime oxygen of amidoxime (I) is placed at a close distance of 1.714 Å from the hydrogen atom of the His447. The docking study reveals the stabilization of the

uncharged reactivator (amidoxime (I)) by the surrounding residues in the active site with non-covalent interactions.

The earlier report with the nucleophilic sites of amidoxime and aldoxime based reactivators suggests that the later one showed better efficacy towards tabun-*h*AChE.[23] We have performed the docking study with these reported reactivators with the crystal structure of tabun-inhibited *m*AChE (pdb code: 2JF0). The approach of both the reactivators towards the electrophilic phosphorus atom of tabun inhibited adduct is very similar in nature. (Fig S3, S4 and S5 in Supplementary Information) Importantly, comparing the docking studies performed with the model amidoxime (I) and the amidoxime based reactivator (8,9) with the tabun-inhibited *m*AChE (pdb code: 2JF0), the model system (I) is relatively at a larger distance from the electrophilic site compared to the reactivators (8, 9).[23] This result qualitatively suggests that the role of alkyl chain length is important in the reactivation process. Our model study although showed the better nucleophilicity for amidoxime compared to aldoxime system, a more quantitative investigation is required with the peripheral sites to understand the difference in efficacy of such oxime drugs.

In the reactivation therapy, the diffusion of reactivators through the blood brain barrier (BBB) is one of the important criterions in the drug design process.[43] Most of the reported oximes having permanent charge are hydrophilic in nature and do not cross the BBB by a simple diffusion through the cell membrane whereas the lipophilic compounds can penetrate easily.[44] Recently, the development of neutral drug like candidates that can easily cross the BBB into the brain due to its lower solubility in water is an active field of research in the reactivation process.[10] Therefore, we have examined the ability of the chosen neutral amidoxime (I) to cross the blood-brain barrier with the help of LogP calculations. The lower LogP values suggest the hydrophilic nature of compounds, whereas the positive values indicate the hydrophobic characteristics.[45] We have used Prologp module of Pallas 3.8.1.2 software to calculate the LogP value of amidoxime (I).[35] The LogP value calculated for amidoxime (I) is higher than the reported mono pyridinium reactivator 2-PAM.[15] (table 1) The higher LogP value of amidoxime (I) indicates its greater capability to cross the BBB for the reactivation of tabun-inhibited AChE in the CNS compared to 2-PAM.

Table 1. The octanol-water partition coefficient (LogP) of 2-PAM and Amidoxime (I).

Oxime	LogP
2-PAM	-2.38
Amidoxime (I)	-0.14

Conclusions

In this article, we have examined the aging and reactivation mechanisms of the tabun-conjugated AChE using post-Hartree-Fock *ab initio* MP2 calculations. The aging process initiated by OH⁻ attacks can proceed via two main mechanisms, O-C bond and P-N bond cleavages. We have examined these two pathways for the aging process as suggested by earlier crystallographic and mass spectrometric analyses of aged tabun-inhibited AChE and BChE. The O-dealkylation mechanism reported for the aging of tabun-inhibited AChE has been computed to be higher energetic process compared to the reactivation process of the inhibited enzyme. The model calculations performed for the cleavage of O-C bond and P-N bond show that P-N deamination mechanism is a catalytic control process and preferred for the aging of tabun-inhibited AChE. The role of protein environment is not considered in these model studies and presumably shows the role of steric and electronic effects in the departure from the observed results. The computation results reveal that the reactivation process can compete with the aging process with amidoxime (I). The energy of activation calculated for reactivation of tabun-conjugated AChE by amidoxime (I) is 2.3 kcal/mol, which is lower than the activation energies calculated for the studied aging processes. The docking results show that amidoxime (I) has been stabilized by non-covalent interactions with favourable orientation of nucleophilic oxygen of the oxime towards phosphate of tabun. Furthermore, the position of protonated histidine and the distance between nucleophile and electrophile reveals the capability of amidoxime (I) to reactivate the tabun-inhibited AChE. The aldoxime as reported to be efficient for the reactivation of tabun-inhibited AChE also showed good results in docking studies. The greater LogP value of (I) indicates the better penetration of neutral reactivator across the BBB for the reactivation process in the CNS than mono pyridiniumoxime 2-PAM. This study sheds light on the reactivation process of OP-inhibited AChE with neutral antidotes prior to the irreversible aging process occurs.

Notes and references

[a]Computation and Simulation Unit (Analytical Discipline and Centralized Instrument Facility), CSIR-Central Salt & Marine Chemicals Research Institute, Bhavnagar, Gujarat, India-364 002.

[b]Academy of Scientific and Innovative Research, CSIR-CSMCRI, Bhavnagar, Gujarat, India-364 002.

Email: ganguly@csmcri.org

Electronic Supplementary Information (ESI) available: [Cartesian coordinates of all the stationary points at M05-2X/6-31G* calculated in this article and the corresponding electronic energies at MP2/6-31+G* level of theory in aqueous phase are available in the supplementary data.]. See DOI: 10.1039/b000000x/

Medicinal Chemistry Communications Accepted Manuscript

References

1   D. Barak, A. Ordentlich, D. Kaplan, R. Barak, D. Mizrahi, C. Kronman, Y. Segali, B. Velan, A. Shafferman, *Biochemistry* 2000, **39(5)**, 1156.

2   E. Elhanany, A. Ordentlich, O. Dgany, D. Kaplan, Y. Segall, R. Barak, B. Velan, A. Shafferman, *Chem. Res. Toxocol.*2001, **14 (7)**, 912.

3   E. Caletti, H. Li, B. Li, F. Ekström, Y. Nicolet, M. Loiodice, E. Gillon, M. T. Froment, O. Lockridge, L. M. Schopfer, P. Masson, F. Nachon, *J. Am. Chem. Soc.* 2008, **130 (47)**, 16011.

4   F. Ekström, C. Akfur, A. K. Tunemalm, S. Lundberg, *Biochemistry* 2006, **45**, 74.

5   W. Jiang, J. R. Cashman, F. Nachon, P. Masson, L. M. Schopfer, O. Lockridge, *Toxicological Sciences* 2013, **132**, 390.

6   E. Carletti, J. P. Colletier, F. Dupeux, M. Trovaslet, P. Masson, F. Nachon, *J. Med. Chem.* 2010, **53**, 4002.

7   F. Nachon, E. Carletti, F. Worek, P. Masson, *Chem. Biol. Interact.* 2010, **187**, 44.

8   E. Carletti, N. Aurbek, E. Gillon, M. Loiodice, Y. Nicolet, J. C.Fontecilla-Camps, P. Masson, H. Thiermann, F. Nachon, F. Worek. *Biochem. J.* 2009,**421**, 97.

9   M. K. Kesharwani, T. Bandyopadhyay, B. Ganguly, *Theor. Chem. Acc.* 2012, **131**, 1175 (1-9).

10 G. Mercey, T. Verdelet, J. Renou, M. Kliachyna, R. Baati, F. Nachon, L. Jean, P.Y. Renard, *Acc. Chem. Res.* 2012, **45**, 756.

11 H. O. Michel, B. E. Hackley, L. Berkowitz, G. List, E. B. Hackely, W. Gillilan, M. Pankau, *Arch. Biochem. Biophys.*1967, **121**, 29.

12 G. S. Sirin, Y. Zhou, L. Lior-Hoffman, S. Wang, Y. Zhang, *J. Phys. Chem. B.* 2012 , **116**, 12199.

13 C. Luo, C. Chambers, N. Pattabiraman, M. Tong, P. Tipparaju, A. Saxena, *Biochemical Pharmacology* 2010, **80**, 1427.

14 Y. Li, L. Du, Y. Hu, X. Sun, J. Hu, *Can. J. Chem.,* 2012, **90**, 376.

15 R. Lo, N. B. Chandar, M. K. Kesharwani, A. Jain, B. Ganguly, *PLOS ONE* 2013, **8(12)**, e79591.

16 G. E. Garcia, A. J. Campbell, J. Olson, D. Moorad-Doctor, V. I. Morthole, *Chem. biol. inter .* 2010, **187**, 199.

17 R. K. Sit, Z. Radić, V. Gerardi, L. Zhang, E. Garcia, M. katalinic, G. Amitai, Z. Kovarik, V. V. Fokin, K. B. Sharpless, P.Taylor, *J. Biol. Chem.* 2011, **286**, 19422.

18 Z. Radić, R. K. Sit, Z. Kovarik, S. Berend, E. Garcia, L. Zhang, G. Amitai, C. Green, B. Radić, V. V. Fokin, K. B. Sharpless, P. Taylor, *J. Biol. Chem.* 2012, **287**, 11798.

19 J. Kalisiak, E. C. Ralph, J. R. Cashman, *J. Med. Chem.* 2012, **55**, 465.

20 J. Renou, M. Loiodice, M. Aerboléas, R. Baati, L. Jean, F. Nachon, P. Y. Renard, *Chem Comm.* 2014, **50**, 3947.

21 G. Saint-André, M. Kliachyna, S. Kodepelly, L. Louise-Leriche, E. Gillon, P. Y. Renard, F. Nachon, R. Baati, A. Wagner, *Tetrahedron* 2011, **67**, 6352.

22 L. Louise-Leriche, E. Păunescu, G. Saint-André, R. Baati, A. Romieu, A. Wagner, P. Y. Renard, *Chemistry A European journal* 2010, **16**, 3510.

23 M. Kliachyna, G. Santoni, V. Nussbaum, J. Renou, B. Sanson, J. P. Colletier, M. Arboléas, M. Loiodice, M. Weik, L. Jean, P. Y. Renard, F. Nachon, R. Batti, *European Journal of Medicinal Chemistry* 2014, **78**, 455.

24 L. Bromberg, H. Schreuder-Gibson, W. R. Creasy, D. J. McGarvey, R. A. Fry, T. A. Hatton, *Ind. Eng. Chem. Res.* 2009, **48**, 1650.

25 F. J. Ekström, C. Åstot, Y. P. Pang, *Clin. Pharmacol. Ther.*2007**, 82**, 282.

26 Y. Zhao, D. G. Truhlar, *Acc. Chem. Res.* 2008, **41**, 157.

27 M. J. Frisch, G. W. Trucks, H. B. Schlegel, G. E. Scuseria, M. A. Robb, J. R. Cheeseman, G. Scalmani, V. Barone, B. Mennucci, G. A. Petersson, H. Nakatsuji, M. Caricato, X. Li, H. P. Hratchian, A. F. Izmaylov, J. Bloino, G. Zheng, J. L. Sonnenberg, M. Hada, M. Ehara, K. Toyota, R. Fukuda, J. Hasegawa, M. Ishida, T. Nakajima, Y. Honda, O. Kitao, H. Nakai, T. Vreven, J. A. Montgomery, Jr, J. E. Peralta, F. Ogliaro, M. Bearpark, J. J. Heyd, E. Brothers, K. N. Kudin, V. N. Staroverov, T. Keith, R. Kobayashi, J. Normand, K. Raghavachari, A. Rendell, J. C. Burant, S. S. Iyengar, J. Tomasi, M. Cossi, N. Rega, J. M. Millam, M. Klene, J. E. Knox, J. B. Cross, V. Bakken, C. Adamo, J. Jaramillo, R. Gomperts, R. E. Stratmann, O. Yazyev, A. J. Austin, R. Cammi, C. Pomelli, J. W. Ochterski, R. L. Martin, K. Morokuma, V. G. Zakrzewski, G. A. Voth, P. Salvador, J. J. Dannenberg, S. Dapprich, A. D. Daniels, O. Farkas, J. B. Foresman, J. V. Ortiz, J. Cioslowski, D. J. Fox (2010) Gaussian 09, Revision B01. Gaussian, Inc, Wallingford, CT.

28 (*a*) E. Cancès, B. Mennucci, J. Tomasi, *J. Chem. Phys.*1997, **107**, 3032 (*b*) B. Mennucci, J. Tomasi, *J. Chem. Phys.*1997, **106**, 5151 (*c*) V. Barone, M. Cossi, J. Tomasi, *J. Chem. Phys.*1997, **107**, 3210.

29 (a) V. Barone, M. Cossi, J. Tomasi, *J. Comput.Chem.*1998, **19**, 404 (b) J. Tomasi, B. Mennucci, E. Cancès, *J. Mol. Struct.(Theochem)*1999, **464**, 211.

30 C. Møller,M. S. Plesset, *Phys. Rev.* 1934, **46**, 618.

31 C. González, H. B. Schlegel, *J. Chem. Phys.*1991, **95**, 5853.

32 D. E. Glendening, A. E. Reed, J. E. Carpenter, F. Weinhold.NBO Version.3.1, 1992.

33 F. Mohamadi, N. G. Richards, W. C. Guida, R. Liskamp, M. Lipton, *J. Comput.Chem.*1990, **11**, 440.

34 Autodock, version 4.2 ed, The Scripps Research Institute: La Jolla, CA, 2007.

35 The Pallas PrologP program is a Trademark of CompuDrug, Inc., www.compudrug.com.

36 C. B. Millard, G. Kryger, A. Ordentlich, H. M. Greenblatt, M. Harel, M. L. Raves, Y. Segall, D. Barak, A. Shafferman, I. Silman, J. L. Sussman, *Biochemistry* 1999, **38**, 7032.

37 G. R. J. Thatcher, R. Kluger, *Adv. Phys. Org. Chem.* 1989, **25**, 99.

38 A. Saxena, C. Viragh, D. S. Frazier, I. M. Kovach, D. M. Maxwell, O. Lockridge, B. P. Doctor, *Biochemistry* 1998, **37**, 15086.

39 E. Heilbronn, *Biochem Pharmacol* 1963, **12**, 25.

40 X. Tang, L. Zhu, J. Chen, J. Hu, Q. Zhang, W. Wang, *Computational and Theoretical Chemistry* 2014, **1035**, 44.

41 F. Worek, H. Thiermann, L. Szinicz, P. Eyer, *Biochemical Pharmacology* 2004, **68**, 2237.

42 J. Cabal, K. Kuča, J. Kassa, *Basic& Clinical Pharmacology & Toxicology* 2004, **95**, 81.

43 M. Remko, A. Boháč, L. Kováčiková, *Struct. Chem.* 2011, **22**, 635.

44 D. E. Lorke, H. Kalasz, G. A. Petroianu, K. Tekes, *Current Medicinal Chemistry* 2008, **15**, 743.

45 R. Lo, B. Ganguly, *Molecular BioSystems* 2014, **10**, 2368.
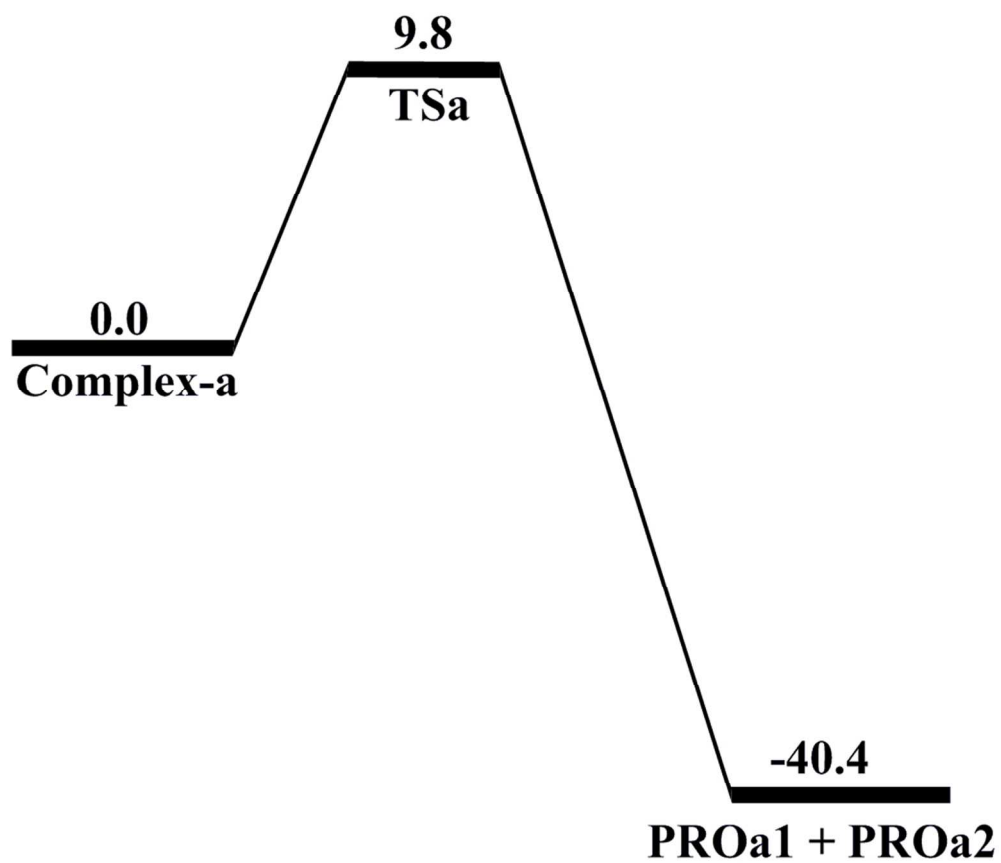
Fig. 1. MP2/6-31+G*//M05-2X/6-31G* calculated energy profile diagram for O-deakylation of tabun-conjugated AChE in aqueous phase. Relative energies are in kcal/mol.
88x77mm (300 x 300 DPI)
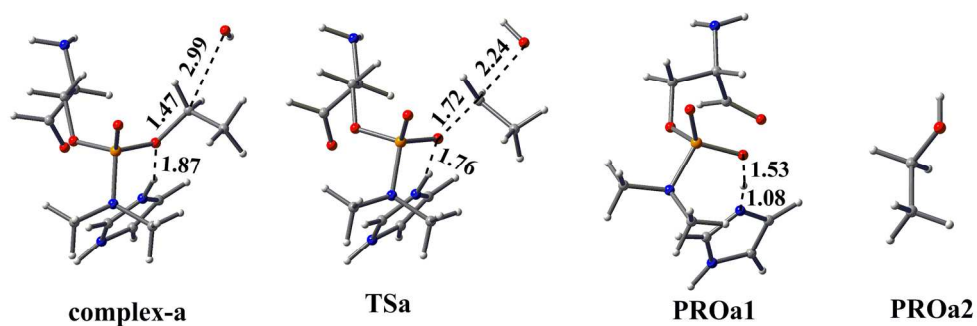
Fig. 2. M05-2X/6-31G* optimized geometries and selected bond distances in Å for species involved in O-dealkylation of tabun-conjugated AChE in aqueous phase (grey= carbon, blue = nitrogen, white = hydrogen, orange= phosphorus and red = oxygen)
171x57mm (300 x 300 DPI)
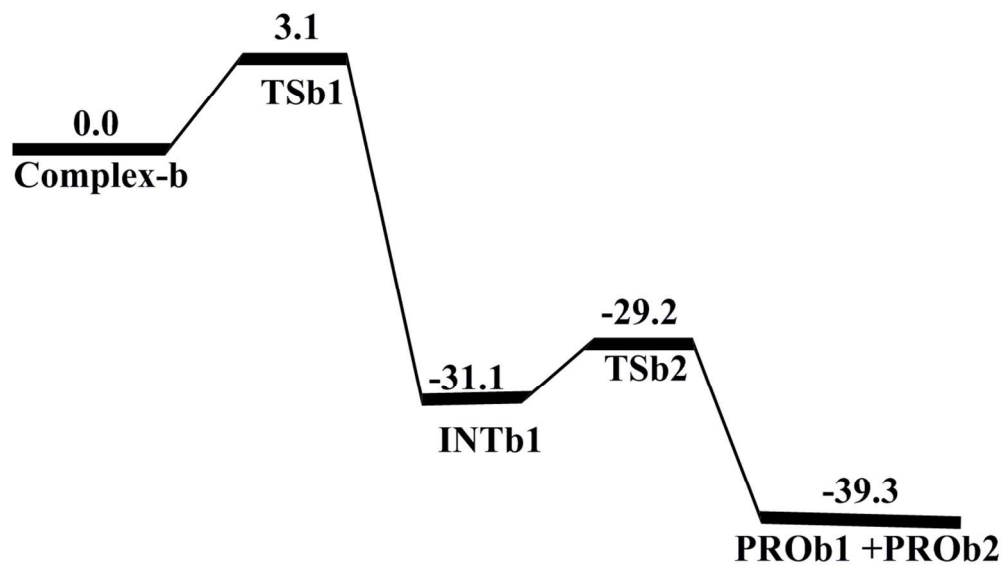
Fig. 3. MP2/6-31+G*//M05-2X/6-31G* calculated energy profile diagram for deamination (P-N anti elimination) of tabun-conjugated AChE in aqueous phase. Relative energies are in kcal/mol.
113x65mm (300 x 300 DPI)
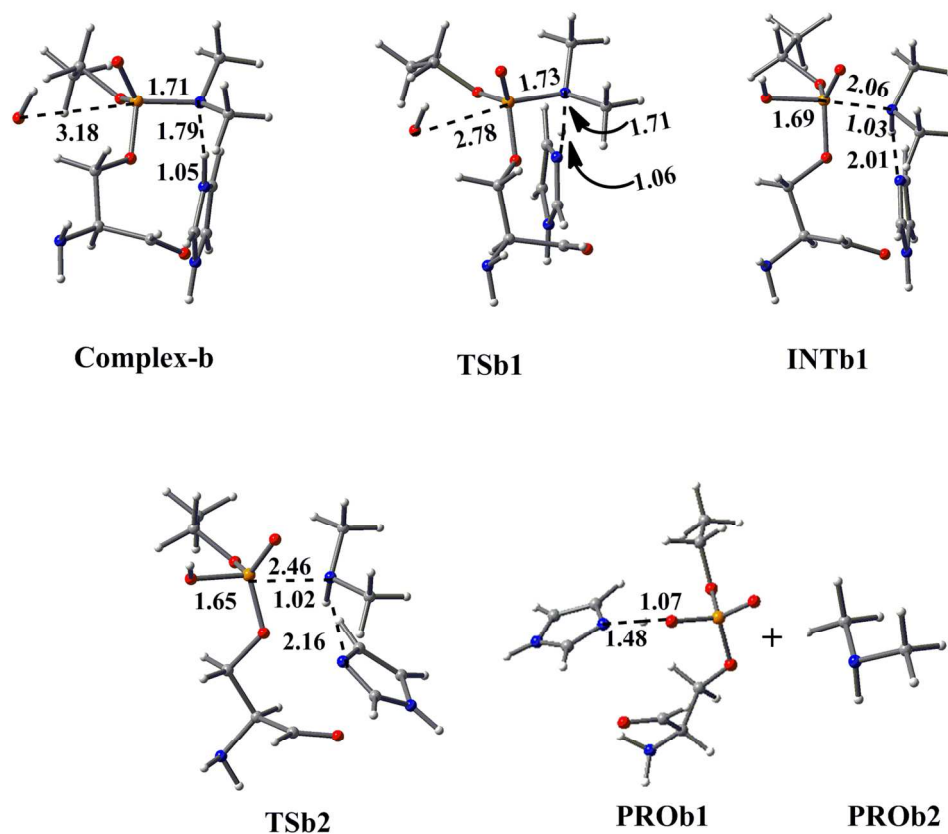
Fig. 4. M05-2X/6-31G* optimized geometries and selected bond distances in Å for species involved in deamination (P-N anti elimination) of tabun-conjugated AChE in aqueous phase (grey= carbon, blue = nitrogen, white = hydrogen, orange= phosphorus and red = oxygen)
136x116mm (300 x 300 DPI)
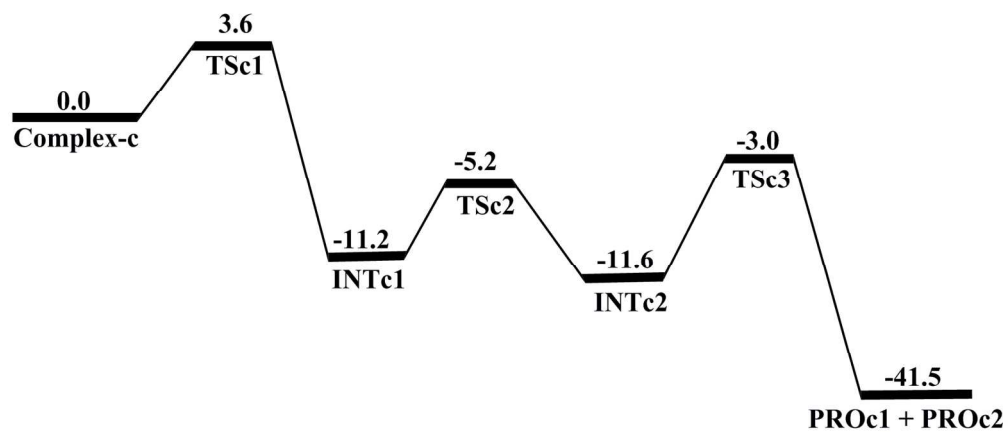
Fig. 5. MP2/6-31+G*//M05-2X/6-31G* calculated energy profile diagram for deamination (P-N rearrangement process) of tabun-conjugated AChE in aqueous phase. Relative energies are in kcal/mol. 154x67mm (300 x 300 DPI)
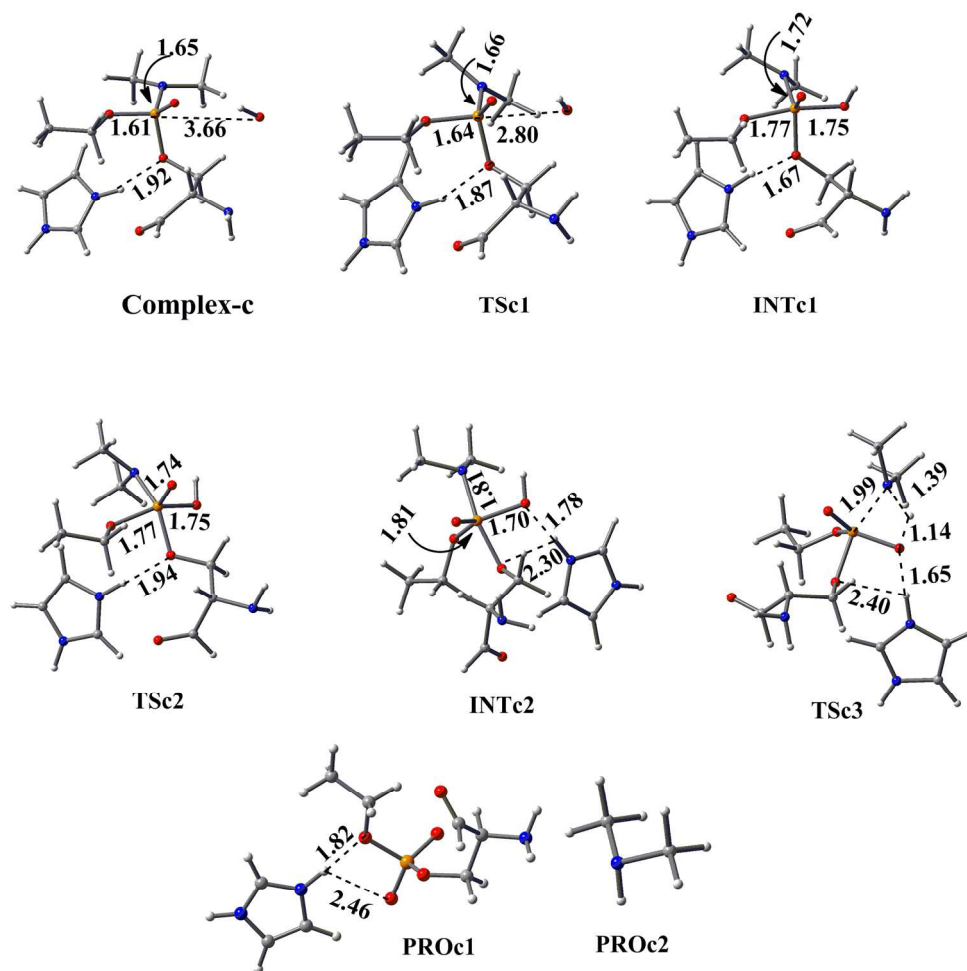
Fig. 6. M05-2X/6-31G* optimized geometries and selected bond distances in Å for species involved in deamination (P-N rearrangement-deamination process) of tabun-conjugated AChE in aqueous phase (grey= carbon, blue = nitrogen, white = hydrogen, orange= phosphorus and red = oxygen).
174x171mm (300 x 300 DPI)
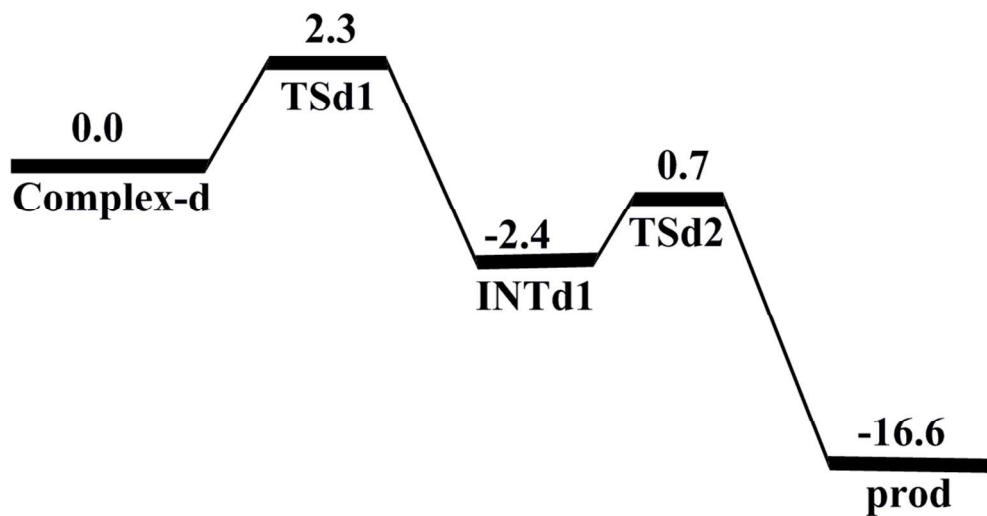
Fig. 7. The potential energy surface for reactivation process of tabun-inhibited AChE conjugate at MP2/6-31+G*//M05-2X/6-31G* level of theory in aqueous phase. Relative energies are given in kcal/mol.
100x52mm (300 x 300 DPI)
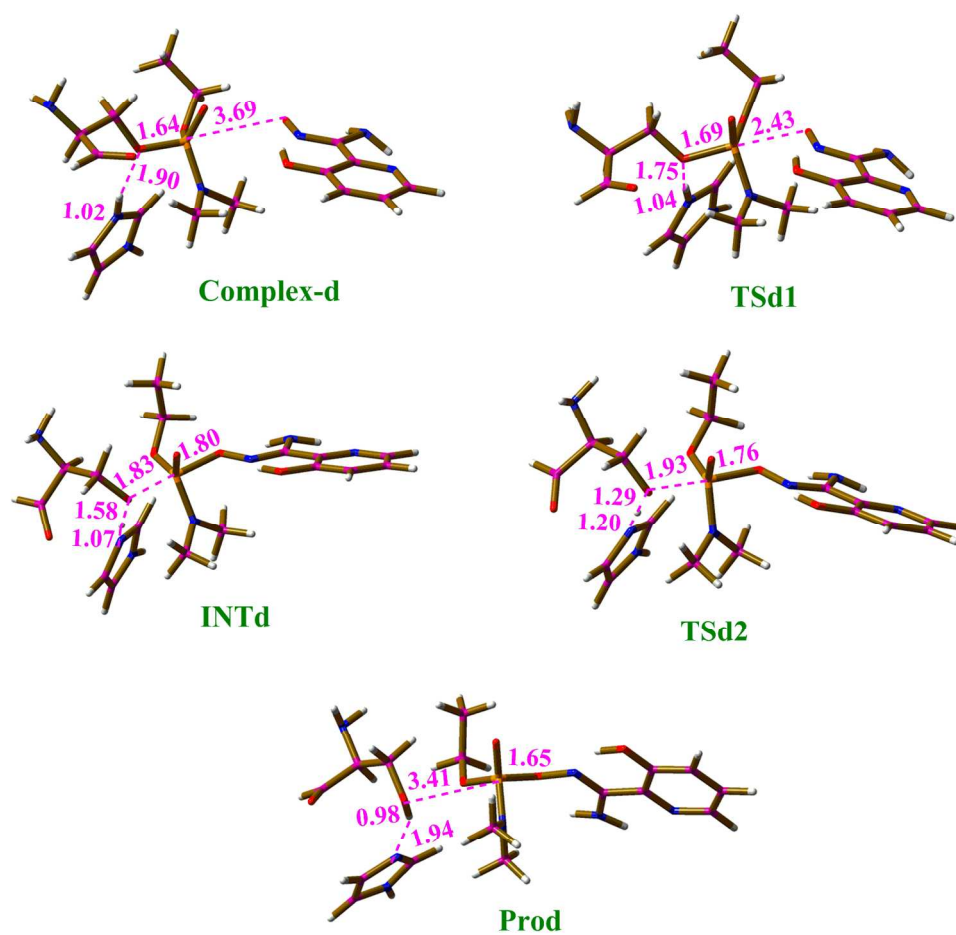
Fig. 8. The optimized geometries and distances are in Å for reactivation process of tabun-inhibited AChE conjugate at M05-2X/6-31G* level in aqueous phase. (red = oxygen, brown = carbon, blue = nitrogen, white = hydrogen)
167x158mm (300 x 300 DPI)
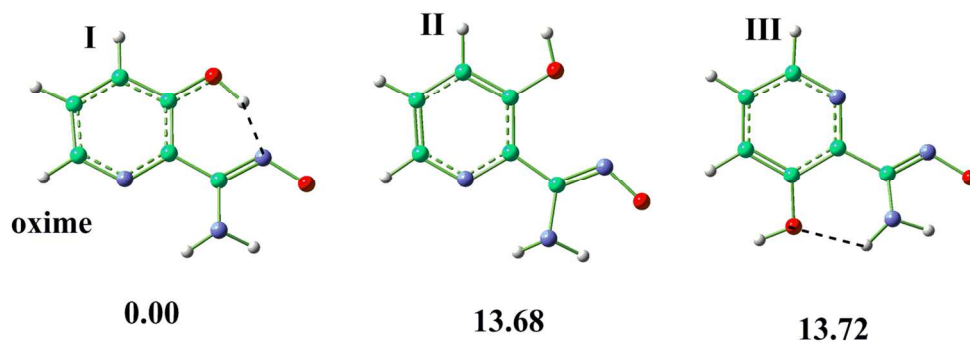
Fig. 9. M05-2X/6-31G* optimized geometries in aqueous phase of various possible conformers of 3-hydroxy-2-Pyridylamide oxime (amidoxime (I)) and their relative energies in kcal/mol at MP2/6-31+G*//M05-2X/6-31G* level of theory. (red = oxygen, green = carbon, blue = nitrogen, white = hydrogen)
132x46mm (300 x 300 DPI)
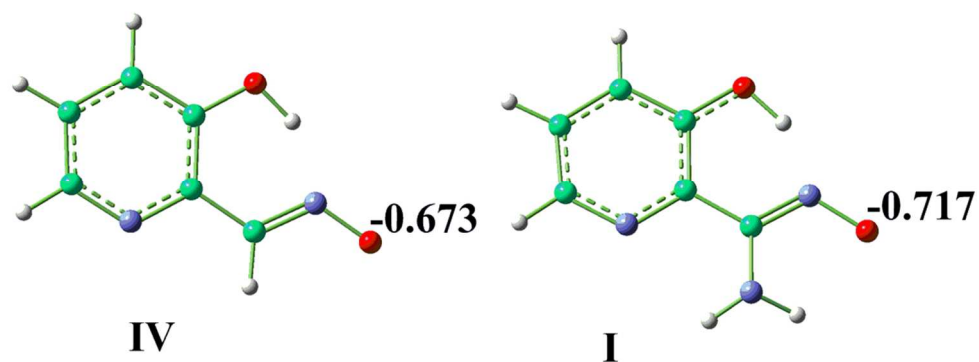
Fig. 10. Optimized geometries in aqueous phase of aldoxime (IV), amidoxime (I) and their NBO charges of active oxygen at M05-2X/6-31G* level of theory. (red = oxygen, green = carbon, blue = nitrogen, white = hydrogen)
100x37mm (300 x 300 DPI)
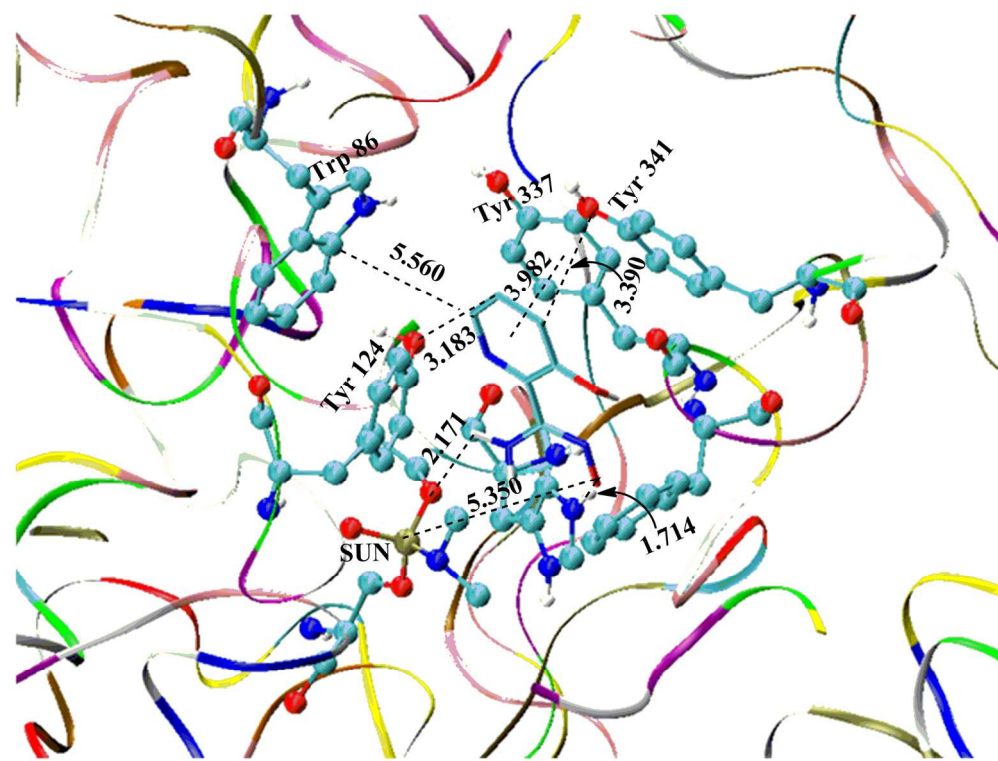
Fig. 11. Stable conformation of amidoxime (I) with tabun-inhibited AChE showing interactions in the active site gorge. (red = oxygen, cyan = carbon, blue = nitrogen, white = hydrogen) (surrounding aromatic residues and SUN are shown in CPK and amidoxime (I) shown in tube format).
163x123mm (300 x 300 DPI)
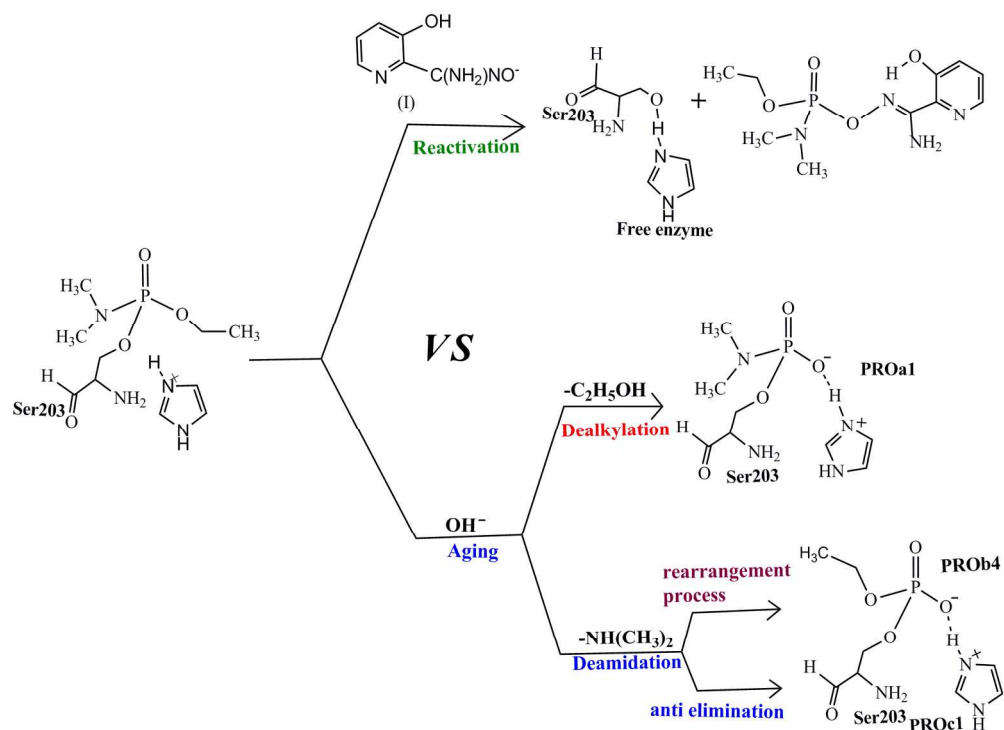
Scheme 1: Schematic representation of possible aging pathways and reactivation pathway of OP-conjugated AChE.
176x128mm (300 x 300 DPI)